Molecular dynamics simulations of threshold displacement energies in Fe

K. Nordlund [a,*], J. Wallenius [b,c], L. Malerba [d]

[a] *Accelerator Laboratory, University of Helsinki, P.O. Box 43, 00014 Helsinki, Finland*
[b] *Department of Nuclear and Reactor Physics, Royal Institute of Technology, Stockholm, Sweden*
[c] *Department of Neutron Research, Uppsala University, Uppsala, Sweden*
[d] *Reactor Materials Research Unit, SCK-CEN, Mol, Belgium*

Abstract

We compare systematically the threshold displacement energy surface of 11 interatomic potentials in Fe. We discuss in detail different possible definitions of threshold displacement energies, and how they relate to different kinds of experimental threshold displacement energies. We compare the threshold results to experiments, and find that none of the 11 tested potentials agrees fully with experiments. However, all the potentials predict some qualitative features in the same way, most importantly that the threshold energy surface close to the 100 crystal direction is flat and that the largest threshold energies occur around very roughly the 123 crystal direction.
© 2006 Elsevier B.V. All rights reserved.

1. Introduction

One of the basic quantities defining the radiation resistance of a material is the threshold displacement energy, i.e. the energy needed to displace an atom in a material to create a stable Frenkel pair. The concept of threshold displacement energy was probably devised by Wigner in the early 1940s, as reported by Burton [1], and already in 1949 it appeared as a functional parameter in Seitz's model to treat elastic collisions [2], where it was assessed as equal to the sum of the cohesive energy plus the formation energy of the Frenkel pair (in total about 25 eV). Since then it has played a key role in radiation damage theory. For example, if the amount of radiation-induced defects increases linearly with energy, the damage level can be well predicted by the Kinchin–Pease (or its variation NRT [3]) equation

which states that the amount of damage is proportional to the ratio of the nuclear deposited energy and an effective threshold displacement energy E_d^* [4]. Even in materials where the Kinchin–Pease equation is not valid, typically dense metals, the damage level is often given in terms of a cascade efficiency which is the actual number of defects compared to the Kinchin–Pease prediction [5,6]. Because of this, it is of importance to know the value of the threshold displacement energy in any material where irradiation effects are of interest.

The threshold displacement energy has been studied both experimentally and by computer simulations in a wide range of materials (see e.g. [7–10] and references therein). From an application point of view, of particular interest is the threshold displacement energy in Fe. Radiation damage in Fe-based materials is of great interest because the main structural materials in fission and fusion reactors are steels. In addition, it is possible to use ion implantation to harden steels. Thus it is surprising that the threshold

---

* Corresponding author. Tel.: +358 919150007; fax: +358 919150042.
  E-mail address: kai.nordlund@helsinki.fi (K. Nordlund).

displacement energy in Fe has in fact been studied less than in many other materials. The average threshold displacement energy most frequently used for Fe, the so-called NRT or ASTM standard, is 40 eV [11]. Its source in literature review papers [7,8] is often cited to be [10], but this paper is also a review and bases its value on the MD simulations carried out by Erginsoy et al. in 1964 [12]. There is one experiment by Lucasson which gives an average threshold energy of 24 eV for Fe [13], but in his later review papers even Lucasson himself does not use this value [10], apparently because the result is dependent on the choice of the damage model. The experiments which do exist give only the threshold energy along the low-index lattice directions 100 [14], 110 and 111 [15,16], not the average over all directions, that would be most appropriate for the effective threshold displacement energy used in the Kinchin–Pease formulation.

There have been significant advances in not only computer capacity but also in the understanding of interatomic interactions since 1964 [17–19], including additional theoretical works on the threshold displacement energy in Fe. Agranovich and Kirsanov [20] studied the threshold energies close to 100 and 111 including thermal displacements (in contrast to the work of Erginsoy et al. that was carried out at 0 K) and obtained threshold energies of 18 eV around 100 and 26 eV around 111, in fairly good agreement with the experiments of Lomer and Pepper [15]. Apparently the first systematic simulations of threshold energies in Fe employing many-body potentials were carried out by Bacon et al. [21] who in 1993 simulated threshold energies with the Finnis–Sinclair potential [17], modified in the repulsive part [22]. They obtained thresholds of 18 eV around 100, 30 eV around 110 and >70 eV around 111 at 0 K. Soon after this, Doan and Vascon [23] adjusted another Fe potential [24] with a repulsive potential in a manner which gave good agreement with experiments [23]: 21 eV around 100, 31 eV around 110 and 18.5 eV around 111. Also several other, less detailed, studies of the threshold displacement energies have been carried out in the context of adjusting the repulsive part of the potentials to have a realistic high-energy part (see Section 2.3). However, none of the works on the threshold energy in Fe have affected the NRT standard. Moreover, the works have used slightly different (and sometimes poorly documented) definitions of what the threshold energy is, especially regarding whether it is calculated in the exact crystallographic direction, or in some angular interval around it to account for electron beam spreading. Hence it is of interest to review the threshold energies given by different models using the same threshold energy definitions for all the potentials.

In the current paper we systematically reexamine the issue of the threshold displacement energy in Fe. We simulate the full three-dimensional threshold energy surface using 11 different interatomic potentials, taking care that all non-physical simulation parameters (such as the simulation cell size) are chosen so that they do not affect the end result. We compare the results of all potentials with each other and experiment. We also discuss the original simulations by Erginsoy et al. in view of the present simulations.

2. Method

2.1. Definition of threshold displacement energy

It might seem to be straightforward to define a threshold displacement energy of a material. However, one can in fact define several different threshold displacement energies depending on the viewpoint and the experimental situation one wishes to model. Since distinguishing between these is important for understanding some of the results of this paper, we review here different possible definitions.

The most straightforward distinction comes from consideration of irradiation geometry. First of all, it is possible to define a direction-specific threshold for each lattice direction, $E_d(\theta, \phi)$. This can be measured by electron irradiation of a thin single crystal specimen [25]. The full function $E_d(\theta, \phi)$ forms the threshold energy surface. An average threshold energy E_d^{ave} can be defined as the average of the function $E_d(\theta, \phi)$ over all angles.

However, this picture is not the end of the story. Because of thermal and zero-point lattice vibrations [26] atoms never reside exactly on perfect lattice sites. Hence even for the exact same lattice direction, it is possible that a given energy sometimes produces a defect, sometimes not. This lead Malerba and Perlado to introduce the concept of lower and upper thresholds, lower (E_d^l) being the value where a defect sometimes is produced, upper (E_d^u) being the one where it is always produced [27]. This definition was useful in their study of SiC, but the quantity E_d^u is problematic in metals where in-cascade annealing can cause all damage to recombine with a non-zero probability even for very high energies. This non-monotonousness of the threshold displacement energy is illustrated in Fig. 1, which shows the probabilities to form at least one defect $P_{def}^i(E)$ for individual directions i. Note that in one of the cases there is sometimes no damage produced even at an energy of almost 600 eV. Animation of these cases showed that this is a dynamic annealing effect, where an interstitial is formed for a short time, but recombines with the vacancy left at the original site of the recoil before the cell has cooled down. From simulations of defect production with all 11 potentials up to 250 eV we found that for a given direction the probability of a uniform defect production curve (i.e. where a defect is always produced above the lower threshold) is in fact only 10%.

Although one could argue that it is the lower threshold which is the true threshold, the realization of the possibility of recombination at high energies has consequences on the definition of the average threshold displacement energy. Namely, one can choose to either take into account or not take into account the events above E_d^l in the calculation of the average threshold energy. That is, if one uses the
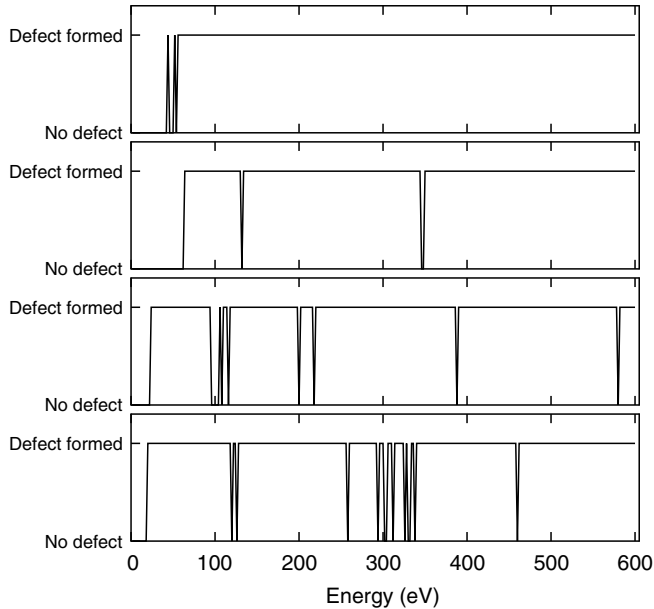
Fig. 1. Probability to form a defect for four recoils in Fe modelled with the ABC potential, as a function of recoil energy. Note that the data illustrates specifically the probability to form *at least* one defect; at the higher energies in many cases more than one defect is formed. In each of the four cases the initial state of the simulation is identical, including identical thermal atom displacements, except for the initial ion energy which is raised in steps of 2 eV.

value of E_d^l only, one can of course calculate the average of this over all angles

$$E_{d,ave}^{av} = \frac{\int_0^{2\pi} \int_0^\pi E_d^l(\theta, \phi) \sin\theta \, d\theta \, d\phi}{\int_0^{2\pi} \int_0^\pi \sin\theta \, d\theta \, d\phi}, \tag{1}$$

where av stands for average. In practice, it is more convenient to select the directions in which the recoils are directed by proper weighting with θ (i.e. ensuring that recoils are generated in equal amounts per solid angle $\sin\theta \, d\theta \, d\phi$), after which the average can be calculated as a direct arithmetic average of the E_d^l values obtained.

To illustrate the probability to form a defect at a given energy, we form the angle-integrated displacement probability function [12] of the E_d^l data. These data are illustrated in Fig. 2, curve 2.

On the other hand, one can also take the average of production probability curves of the form shown in Fig. 1, $P_{def}(E) = ave_i P_{def}^i(E)$. This gives another angle-integrated displacement probability curve, which is illustrated in Fig. 2, curve 1. Note the marked difference between curves 1 and 2: while both start out about similar for low energies, curve 1 has a much slower rise to the maximum of one at high energies. This is because curve 1 accounts for the possibility *not* to form a defect above E_d^l, which lowers the probability. The average threshold energy $E_{d,ave}^{pp}$ (pp stands for production probability) of this data can be calculated in the usual statistical way as

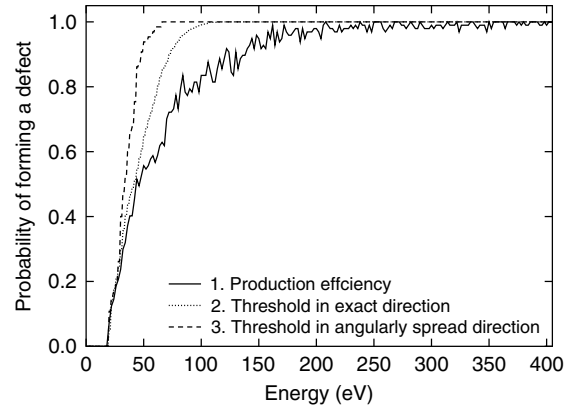$$E_{d,ave}^{pp} = \int_0^\infty E \, dP_{def}(E). \tag{2}$$

Fig. 2. Probability to form a defect at a given energy calculated in three different ways (see text) with the ABC potential.

The threshold concepts introduced until now are well-defined from a mathematical and atomistic point of view. They do not, however, account for one significant experimental complication. When a single-crystalline sample is irradiated with electrons, the electron beam spreads in the sample due to scattering. This effect can be substantial, for instance in [28] a beam spreading of 20° is mentioned. If beam spreading occurs, then it is no longer possible to define a lower threshold E_d^l in an exact lattice direction, such as, say, [3 2 1]. Instead, one needs to define the threshold over some angular or Miller index interval, because it is possible that the scattered electrons find a lower threshold value next to the desired ideal Miller index, say e.g. at [2.94 2.03 1.02] rather than [3 2 1].

It is non-trivial to predict the electron beam spreading in a sample, and the result depends on the exact experimental setup (electron energy, beam spreading in the irradiating beam before it hits the foil and foil thickness). Hence there is no general way in which one can account for this effect, and determining it even for exactly known experimental conditions would require simulation of the electron beam scattering in the material. In the present paper we will use a simple approach to give an estimate of how much this could affect the threshold results. To obtain the angular minima around the low-index lattice directions 1 0 0, 1 1 0 and 1 1 1 reported in Table 1, we use an interval of Δ0.2 Miller index to roughly correspond to the reported 20° spreading.

We also tested the effect of beam spreading for all directions by determining an average threshold for the ABC potential by first taking the minimum of the E_d^l data in each Δ0.1 Miller index interval, i.e.

$$E_d^{l,min} = \min_{0.1 \text{ Miller index interval}} (E_d^l) \tag{3}$$

then getting the average of the $E_d^{l,min}$ data using Eq. (1) to give $E_{d,ave}^{ma}$ (ma stands for minimum in angular window). The effect of this is illustrated in Fig. 2, curve 3. Since now the lowest value in each interval is taken, naturally the threshold energies are reduced.

K. Nordlund et al. / Nucl. Instr. and Meth. in Phys. Res. B 246 (2006) 322–332

325

Table 1
Threshold displacement energy results obtained with the different potentials

Potential	$N_{\text{directions}}$	$E_d(\theta,\phi)$				$E_{d,\text{ave}}^{\text{av}}$	$E_{d,\text{med}}^{\text{av}}$
		All	1 0 0	1 1 0	1 1 1		
ERG	2512	9	9	25	17	22.0 ± 0.2	21
ERG, $a = 2.86$ Å	7280	15	15	33	25	40.4 ± 0.2	41
ABC	3049	17	17	31	35	44.8 ± 0.4	41
WOL	2284	21	21	27	31	40.8 ± 0.3	37
COWP	2386	19	19	47	29	53.5 ± 0.5	53
MHS[a]	13,152	15	15	27	25	36.9 ± 0.1	35
AMS[a]	2699	15	17	33	33	39.0 ± 0.3	35
SP-RB	30,126	15	15	27	19	42.4 ± 0.1	43
HA-VD	2948	19	19	27	19	33.4 ± 0.2	31
HV-TB	3118	17	19	35	19	46.3 ± 0.3	45
JO-GA-SdlR	15,581	15	15	25	29	36.7 ± 0.1	33
FS-CB	4212	15	15	27	29	38.6 ± 0.3	35
Experiment[b]		16–18					
Experiment[c]		17	17	>30	20		
Experiment[d]		20	20	30			

The potential abbreviations and references to them are given in the text. The direction-specific thresholds $E_d(\theta,\phi)$ were obtained as the minimum in an 0.2 Miller index interval around the principal direction to account for beam spreading. The uncertainty of $E_d(\theta,\phi)$ and $E_{d,\text{med}}^{\text{av}}$ are ± 1 eV because the thresholds were determined with an energy step size of 2 eV (hence e.g. a value of 17 eV means that a defect was detected for 18 eV but not 16 eV recoils). The average threshold $E_{d,\text{ave}}^{\text{av}}$ is obtained as an average of direction-specific thresholds $E_d(\theta,\phi)$ for exact angles. $N_{\text{directions}}$ is the number of directions for which a threshold was simulated.

[a] MHS and AMS differ from each other only slightly in the embedding energy part.
[b] Direction-independent experiment [13].
[c] Direction-specific experiments [16].
[d] Direction-specific experiments [15].

We also note that for all of these methods of getting the threshold displacement energies, one can either characterize the distribution with the average, as described above, or the median which is obtained from the data in Fig. 2 as the point where the curves cross the probability 0.5.

All of the threshold energy definitions described in this section are mathematically well defined, and all except the last version $E_{d,\text{ave}}^{\text{ma}}$ are independent of the experimental method used to measure them. Which one should be used depends on the purpose of the study.

For direction-specific threshold energies one should consider $E_d(\theta,\phi)$. In most cases direct measurements of the threshold energies measure the lowest electron energy at which a defect signal (measured e.g. by resistivity) is observed. In this case the relevant threshold is E_d^l. In comparing to experiments, the beam spreading should be included in the consideration.

The average thresholds are typically used in connection with the Kinchin–Pease or NRT equations as estimates of damage levels produced in collision cascades. Then the beam spreading issue is irrelevant and one should use either $E_{d,\text{ave}}^{\text{pp}}$ or $E_{d,\text{ave}}^{\text{av}}$ or the corresponding medians. At first sight, one might think that one should account for the high-energy events not producing defects in the choice, i.e. use $E_{d,\text{ave}}^{\text{pp}}$. However, the effect leading to no defects being produced is in-cascade recombination, the very same effect causing the Kinchin–Pease equation not to be valid in metals at high energies. Hence using $E_{d,\text{ave}}^{\text{pp}}$ for metals could to some extent be considered circular reasoning. This leaves

us to consider the quantity $E_{d,\text{ave}}^{\text{av}}$ (the average of all E_d^l values) as the most appropriate choice of the effective threshold displacement energy E_d^*.

2.2. Simulation method

The points raised in the above discussion are important to realize in choosing a method to simulate the full threshold energy surface. If one wishes to simulate $E_{d,\text{ave}}^{\text{av}}$, one should obtain E_d^l for all lattice directions, i.e. the full function $E_d^l(\theta,\phi)$. To determine this function, one should of course simulate thresholds in all directions.

For each direction, one then picks an atom and gives it a recoil energy in this direction. Because atoms have thermal or zero-point vibration displacements from their lattice sites, each atom position is unique even in a Bravais lattice, and one should either generate new thermal displacements before each event, or choose the initial atom randomly from among several different lattice sites. We used the latter method, choosing the atom position randomly from within the middle eight unit cells of the simulation cell. Comparison with a smaller choosing region indicated this was enough for 'randomization' of the initial position. We tested how large the effect of the initial displacements can be by simulating the threshold for different atoms in the exact same direction. We obtained for five events thresholds between 32 eV and 42 eV, showing that this is a quite substantial effect. If one would want to determine E_d^l in a given direction, one needs to account for this, but

on the other hand if one takes the minimum over an angular or Miller index interval (as discussed above) it becomes automatically taken into account. If one wishes to simulate an average threshold energy $E_{d,ave}$, one should include all E_d^l values for non-equivalent atoms. This is because in cascades recoils are given to atoms with all kinds of thermal displacements.

Since the threshold energy is not monotonously rising, as described above, one cannot use binary search between 0 and a high energy to find efficiently the minimum E_d^l for the given direction. Instead it is necessary to do an exhaustive stepwise search in energy from 0 eV upwards to be certain of finding the correct E_d^l for a specific $(atom, \theta, \phi)$ combination. When a defect-producing event is found, $E_d^l(atom, \theta, \phi)$ is determined and the simulations can be restarted for a new atom and direction. We chose to carry out this search in steps of 2 eV, and simulating at least 2000 combinations of randomly chosen $(atom, \theta, \phi)$ events for each potential studied.

We also carried out another set of runs, where the simulations were not stopped when E_d^l was found, but always continued until an ion energy of 250 eV (600 eV for the ABC potential). These simulations were used to determine the defect production efficiency discussed above for the ABC potential, and the average production of defects used in Section 3.4.

In total the simulations amounted to several million separate MD recoil event simulations for the 11 potentials tested.

The molecular dynamics method used in the simulation of the atom motion of the recoils has been described in detail in previous works and hence we only mention here a few central features. The cells were equilibrated to zero pressure and 36 K temperature by first running an equilibration run with Berendsen temperature and pressure control [29] for 6 ps prior to the start of the recoil simulations. The initialized atom positions and velocities were read in at the beginning of each recoil simulation. Electronic stopping [30–32] is not included in the calculation because the energies used are so low. The system size was 4608 atoms; we also tested a simulation cell size of about 1500 atoms, and found that there was no statistically significant difference between the 1500 atom and 4608 atom cell results, giving confidence the size of 4608 atoms is sufficient. The simulation time was 6 ps per event; visual observation of the atom dynamics and monitoring of the temperature in the cell showed that at this time the cell had cooled down to the original ambient temperature of 36 K (chosen because it was also used in [16]). The simulation cell size of $(12 \times 12 \times 16)$ unit cells was specifically chosen to be non-cubic to reduce the possibility of 111 crowdion interstitial self-interaction around the periodic cell borders. Temperature cooling [29] at the borders was carried out over a region of one unit cell on each side of the cell border with a time constant of 70 fs, while the simulation cell shape and volume was held fixed at the value obtained from the equilibration run.

To detect the defects automatically, we used a combination of two methods. Criterion 1 was to flag a defect if the final potential energy after a recoil event in the cell was more than 4 eV above the average energy in it at thermal equilibrium at 36 K. Criterion 2 was based on a Wigner–Seitz defect analysis [33]. If both of these criteria indicated presence of a defect, a defect was considered detected. If one but not the other of the criteria was fulfilled, a defect was also considered to be detected, but a warning was issued. This can happen e.g. if a defect is just about to recombine at the end of the simulation, or if large fluctuations in potential energy still exist at the end of the simulation. The amount of this kind of warnings was for all potentials less than 1% of all simulated events, giving confidence that the simulation time of 6 ps was long enough.

2.3. Potentials used

The following Fe potentials were considered in this work, listed in the order in which the simulations were carried out. Some of the potentials are part of a potential development effort for Fe compounds, in which case we only used the pure Fe part. In some cases the original potential was modified to include a high-energy repulsive part, in which case we mention it here. Usually the repulsive potential is either the repulsive potential by Biersack and Littmark [34] or the very similar "universal ZBL" repulsive interatomic potential [30]. The potential abbreviations given below are consistent with those used by Malerba in recent related work [35,36].

The pair potential used by Erginsoy et al. in [12], which we label "ERG". The potential by Ackland et al. [37], which we label "ABC". The Fe part of the recent FeCr potential developed by us, which we call "WOL" [38]. The potential developed by Chakarova et al. [39] ("COWP"). The potential number 2 of Mendelev et al. [40] ('MHS') as well as its modification number 10 by Ackland et al. [41] ("AMS"). These two differ only in the embedding energy part. The potential of Simonelli et al. [42], with the repulsive part modified by Becquart et al. [43,44] ("SP-RB"). The potential of Haftel and Andreadis [24], with a repulsive potential added by Doan and Vascon [23] ("HA-VD") The potential of Harrison et al. [45], with the repulsive part modified by Becquart et al. [43,44] ("HV-TB"). The Oh–Johnson potential [46], to which a repulsive part was added by Soneda et al. [47] ("JO-GA-SdlR"). And finally the Finnis–Sinclair Fe potential [17], which was modified in the repulsive part by Calder et al. [22] ("FS-CB"). For those potentials for which the repulsive potential addition was not mentioned, the modification was done by the original potential constructors themselves. All potentials except ERG are three-body potentials with an embedding, but no angular terms.

All of these were realized by us in the form of numerical tables which were read into the MD code "parcas" [33,48] in the original EAM "u3" potential format [49]. The
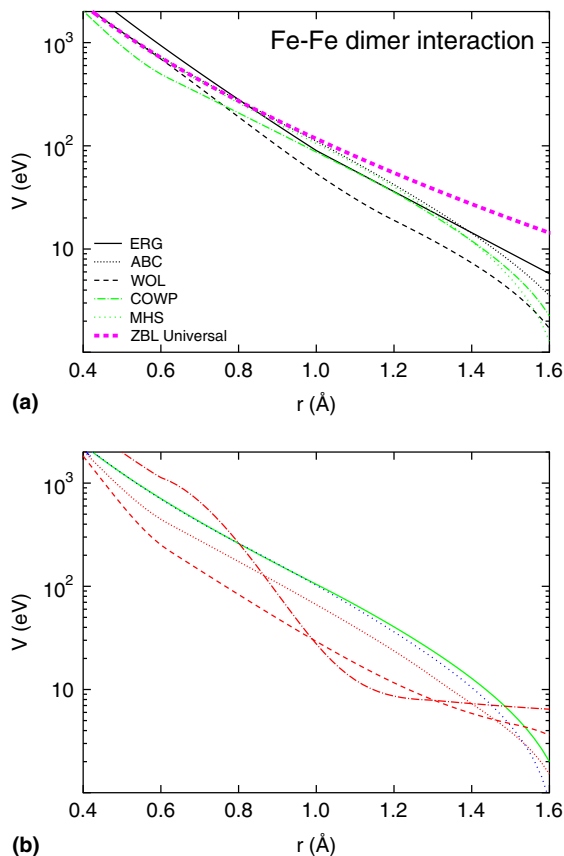
Fig. 3. Repulsive part of all potentials considered in this study, calculated as the total for an Fe_2 dimer. The potential abbreviations and references to them are given in the text. For clarity the figure is split in two parts.

interpolation was done and the forces obtained using cubic spline interpolation [50].

In Fig. 3 we illustrate the repulsive part of the potentials. Almost all of the potentials reach the same value at high energies because they have been joined to the ZBL universal repulsive potential [30]. Interesting, however, is the high variation in the energy/distance range where the joining has been done, and the form that the potential has, in this range. This clearly illustrates the subjective approach many groups (including ourselves) have taken to the joining. Since this energy range is the one that determines the values of the threshold energies, the results suggest greater care should be taken at this part in the future e.g. by fitting the low-energy repulsive part to density functional theory data. Note also that also the many-body ("embedding") part of the potential affects the strength of the interaction in this energy regime, which may increase the variations further.

3. Results and discussion

3.1. Results for different threshold definitions

We used the Ackland potential ("ABC") to test how the different threshold definitions described above affect the

result quantitatively. We obtained values of $E_{d,ave}^{pp} = 63 \pm 1$ eV, $E_{d,ave}^{av} = 44.8 \pm 0.4$ eV, and $E_{d,ave}^{ma} = 32.4 \pm 1.2$ eV. The corresponding median values are $E_{d,med}^{pp} = 44$ eV, $E_{d,med}^{av} = 41$ eV, and $E_{d,med}^{ma} = 33$ eV. The differences in the values can be understood as follows. The "ma" values are always the lowest because they are based on the minimum in an interval. The "pp" values are the largest because high-energy events not producing defects are taken into account (leading to the asymmetry seen in Fig. 2). This is especially well visible in the large difference between the median and average energy for case pp; the asymmetry leads to a strong shift of the average upwards.

The value for $E_{d,ave}^{ma} = 33.4 \pm 1.2$ was obtained with a Miller index interval of 0.1. For the same data an interval of 0.02 gives 42.0 ± 0.5 and an interval of 0.01 gives 43.8 ± 0.5. Comparison of these values with the value of $E_{d,ave}^{av} = 44.4 \pm 0.4$ eV calculated with no angular window indicates that in electron irradiation experiments one can assume that the threshold results correspond to the exact lattice directions if beam spreading effects are of the order of roughly 1° or less.

We also compare these average results with the direction-specific ones given in Table 1. We see that the average of the minima in the 1 0 0, 1 1 0 and 1 1 1 directions is 30 eV, clearly less than any of the true averages. Inspection of the results of the other potentials in the table also show that none of the low-index direction results strongly correlate with the averages.

These large variations show that it does matter in which way the average threshold is calculated, and one should be careful to do it in a manner which best suits the purpose at hand, as well as clearly define in which way it was done to make later comparison with other works possible.

3.2. Results of the erginsoy potential

We tried to reproduce the original results of Erginsoy et al. by reconstructing their pair potential [12]. This potential is a composite of a screened Coulomb, Born–Mayer and Morse potential, but restricted in range to first and second nearest neighbours only. An exact reproduction of these simulations was impossible, however, because instead of the nowadays customary periodic boundary conditions used in MD simulations [51], Erginsoy et al. had surfaces in the cell. These were stabilized by so-called surface forces, which are not well documented [12]. When we used the pair potential given by Erginsoy et al., together with periodic boundary conditions and relaxed the pressure in the system to 0 pressure, we found that the lattice constant obtained was about 7% larger than in experiments (3.07 Å versus 2.86 Å). The cohesive energy of the system is much too weak, about 1.4 eV for the equilibrium lattice constant of 3.07 Å and 1.2 eV for the experimental value of 2.86 Å. The experimental value for Fe is about 4.3 eV [52], so the value by Erginsoy et al. is more than a factor of three off. Comparison with the Girifalco–Weizer potential [53] (also tested by Erginsoy et al.) showed that the reason

the potential energy is so low is the lack of long-range interactions: in the Girifalco–Weizer Morse potential a cut-off of 8.0 Å gives a realistic cohesive energy of about 4.2 eV, but restricting this potential to nearest and second-nearest neighbours reduces the cohesive energy to 2.2 eV (for the same lattice constant).

Since the potential gives clearly too weak cohesion and is thus elastically soft, also the threshold energies are very low, see Table 1. Since Erginsoy et al. report obtaining a good description of the lattice constant (contrary to our finding using pressure relaxation), we infer that the surface forces stabilized the simulated system to a realistic lattice constant, which, however, put the inner parts of the system under a large compressive stress. Our simulations show that this stress is about 300 kbar. This will naturally increase the simulated threshold energies. Table 1 also shows results for the potential of Erginsoy et al. obtained by forcing the system to the experimental lattice constant of 2.86 Å. The direction-specific values of 15, 37 and 25 eV are close to the values of 17, 34 and 38 eV reported by Erginsoy et al., but still do not fully agree.

These results show that the much used "NRT standard" threshold energy for Fe of 40 eV is based on molecular dynamics simulations which cannot be fully reproduced and were carried out in a system under a very high pressure. To put things into perspective, we nevertheless emphasize that the simulations of Erginsoy et al. were a remarkable achievement in 1964 when the MD method itself was only some 5 years old, and computer capacity was extremely limited compared to today's standards.

3.3. Results of many-body potentials

Table 1 presents the results obtained for the different potentials considered in this study. The results shown are compared to threshold energies reported by others in [36] for the COWP, FS-CB, HA-VD, HV-TB, JO-GA-SdlR and SP-RB potentials. The results agree within a couple of eV in almost all cases. The differences found are most likely due to a different angular window, which as discussed above can have a large effect on the results.

The results in Table 1 are interesting both in terms of where they agree with each other, and where they do not.

All potentials except HV-TB give a minimum threshold energy near the 100 direction, with values ranging between 15 and 21 eV. This good agreement is not a coincidence, as almost all authors adjusting the repulsive part of the potential have done that with the experimental threshold value of about 17 eV in mind.

In the direction-specific thresholds for 110 and 111, there are large variations between the potentials. For the 110 direction the minimum threshold is 27 and maximum is 47, while for 111 the range is from 19 to 35. Noteworthy is that considering all three directions, none of the potentials agree with the experimental values of 16–20, $\geqslant 30$ and 20 eV [13,15,16]. The HV-TB potential would seem to come close, but its minimum does not lie in the 100

direction. Moreover, as is evident from Fig. 3, the high-energy repulsive part of this potential is quite unrealistic. The potential which is closest to experiments is SP-RB, which is one of the few potentials which gives a clearly stronger threshold in the 110 than 111 direction, in agreement with experiments. Its minimum threshold energy of 15 eV is also rather close to the experimental values of 16–20 eV [13,16]. The MHS and AMS potentials (which are among the few potentials which predict that the 110 dumbbell is the most stable interstitial structure in agreement with recent density-functional theory works [54]) are in reasonable agreement with experiments except that both predict a too high threshold in the 111 direction.

The average thresholds are in relatively better agreement with each other, as they range from 33 to 53 eV, and all but two of the potentials are in the even narrower range 36–46 eV. The average of all the many-body potential average thresholds is 41 ± 2, in perfect agreement with the NRT standard value of 40 eV. This should not, however, be interpreted to corroborate the NRT standard threshold value. First, since most authors constructing Fe potentials and adjusting its high-energy part have been aware of the value of 40 eV, this may have guided the potential construction. Second, although we find this possibility unlikely, one cannot rule out the possibility that all classical potentials would suffer from a similar systematic error. Hence although the present results certainly support the use of 40 eV as the average threshold displacement energy in Fe, it still would be valuable if new experiments could be carried out to verify whether the value of 40 eV is indeed appropriate.

3.4. Defect production efficiencies compared to experiments

We also compared our results with the experimental defect production efficiencies obtained for polycrystalline Fe in [13]. This was done by integrating the relativistic differential cross section $d\sigma(T)$ with the displacement probability of primary recoil atoms $P_d(T)$

$$\sigma_d(E) = \int_0^{T_m} P_d(T) \, d\sigma(T). \tag{4}$$

Here T_m is the relativistic expression for the maximum energy transfer from an electron of energy E to an atom [55], and $d\sigma(T)$ is given by the McKinley–Feshbach approximation [56], Eq. (20) in [13]. The integral is over the atom recoil energy T. Because T_m and $d\sigma(T)$ are functions of the electron energy E, so is σ_d. Since the maximum electron energy used in the experiments was 1.35 MeV [13], the experimental and thus also simulated data was normalized to $\sigma_d(1.35 \text{ MeV})$.

Lucasson carried out this integral by assuming some shapes for $P_d(T)$ and adjusting the parameters to fit experiments. We can now instead take $P_d(T)$ from the MD simulations as a fixed quantity for each potential. By numerically integrating Eq. (4), using MD data for $P_d(T)$, we obtain a $\sigma_d(E)$ curve which can be directly compared

to experiments, without the need for any adjustable parameters.

The remaining complication is which threshold data should be used for $P_d(T)$. Since the experiments were carried out on polycrystalline Fe, angular beam spreading is not an issue. On the other hand, the experiments measured the Frenkel pair resistivities, which means that if a recoil produces more than one defect, this should be taken into account in the analysis. Hence we believe the most appropriate function to use for $P_d(T)$ is simply the average number of Frenkel pairs produced as a function of recoil energy, $N_{FP}(T)$. We obtained this quantity by summing up the number of vacancies detected in the Wigner–Seitz defect analysis.

In practice, since the maximum recoil energy is now only 123 eV (corresponding to the electron energy 1.35 MeV) and the integral giving $\sigma_d(E)$ always starts from $T = 0$, the results are dominated by the lowest energies.

The results are illustrated in Figs. 4 and 5. Fig. 4 shows the average number of defects produced for the different potentials as a function of recoil energy T. Fig. 5 shows the normalized σ_d calculated using this data and Eq. (4) compared to experiments. The figure shows that the defect production efficiency of the WOL and HV-TB potentials clearly disagree with experiment, while the MHS, SP-RB,

Fig. 5. Atom displacement cross sections $\sigma_d(E)$ normalized to the value at 1.35 MeV, as a function of average electron beam energy E. The squares show experimental data from [13]. The lines show theoretical results obtained by converting MD simulations of defect formation probability $N_{FP}(T)$ into displacement cross sections using the McKinley–Feshbach equations (see text) [56]. For clarity the figure is split in two parts.

JO-GA-SdlR, and FS-CB potentials show good agreement. These results are related to the minimum threshold. As explained above, the results are dominated by the lowest energies. The too small $\sigma_d(E)$ values of the WOL potentials is related to the high threshold, while that of the HV-TB potential is related to the slow rise of the N_{FP} data just after the threshold seen in Fig. 4.

3.5. Contour plots of $E_d(\theta, \phi)$

Fig. 6 shows contour plots of the three-dimensional threshold displacement energy surface obtained from the MD simulations for the SP-RB and MHS potentials. Also shown as an inset is the threshold map of Erginsoy et al. [12]. The map of Erginsoy et al. has much smoother curves than ours, even though they reported simulating only a few hundred events, while for the SP-RB potential we simulated more than 30,000. The source of this discrepancy is not clear to us.

Comparison of the SP-RB and MHS displacement maps shows that even the qualitative features of the displacement energy surfaces differ strongly. A few common features can be noted, however. Both potentials show a relatively
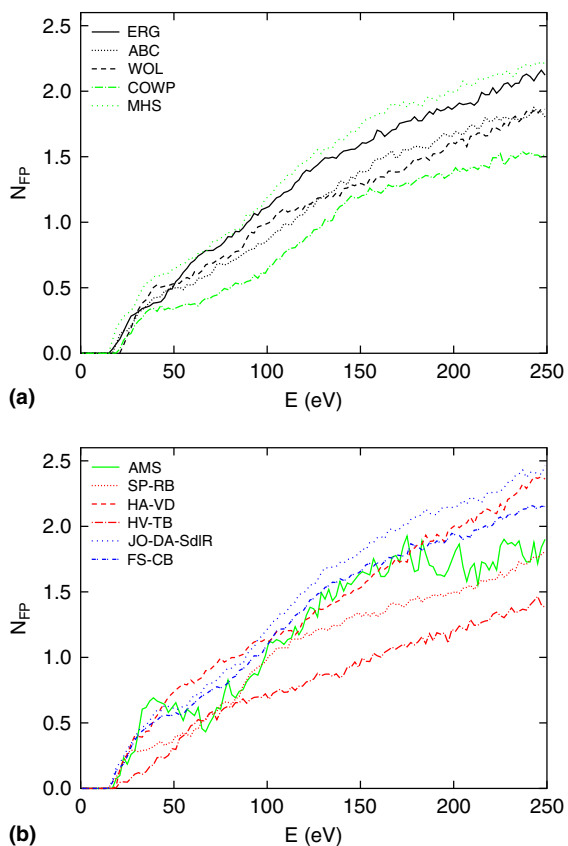
Fig. 4. Average number of defects produced as a function of recoil energy $N_{FP}(T)$ for the different potentials. For clarity the figure is split in two parts.
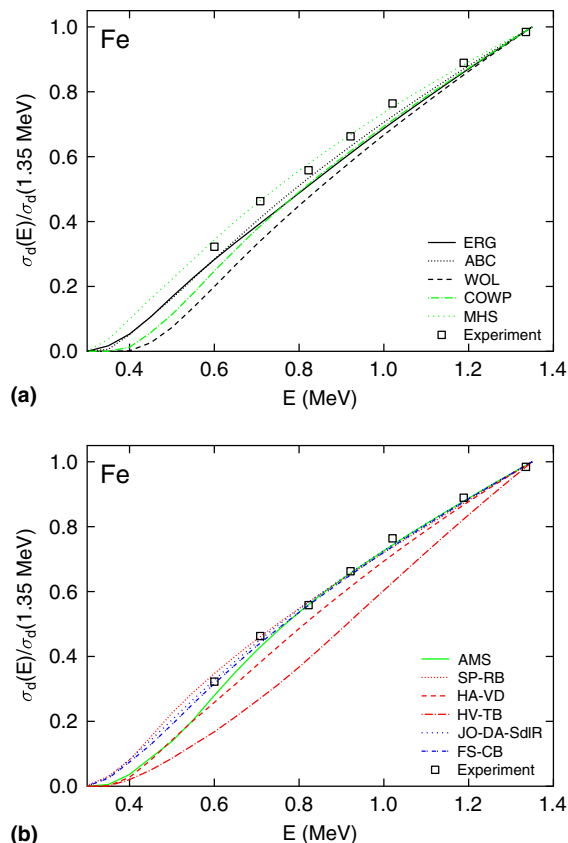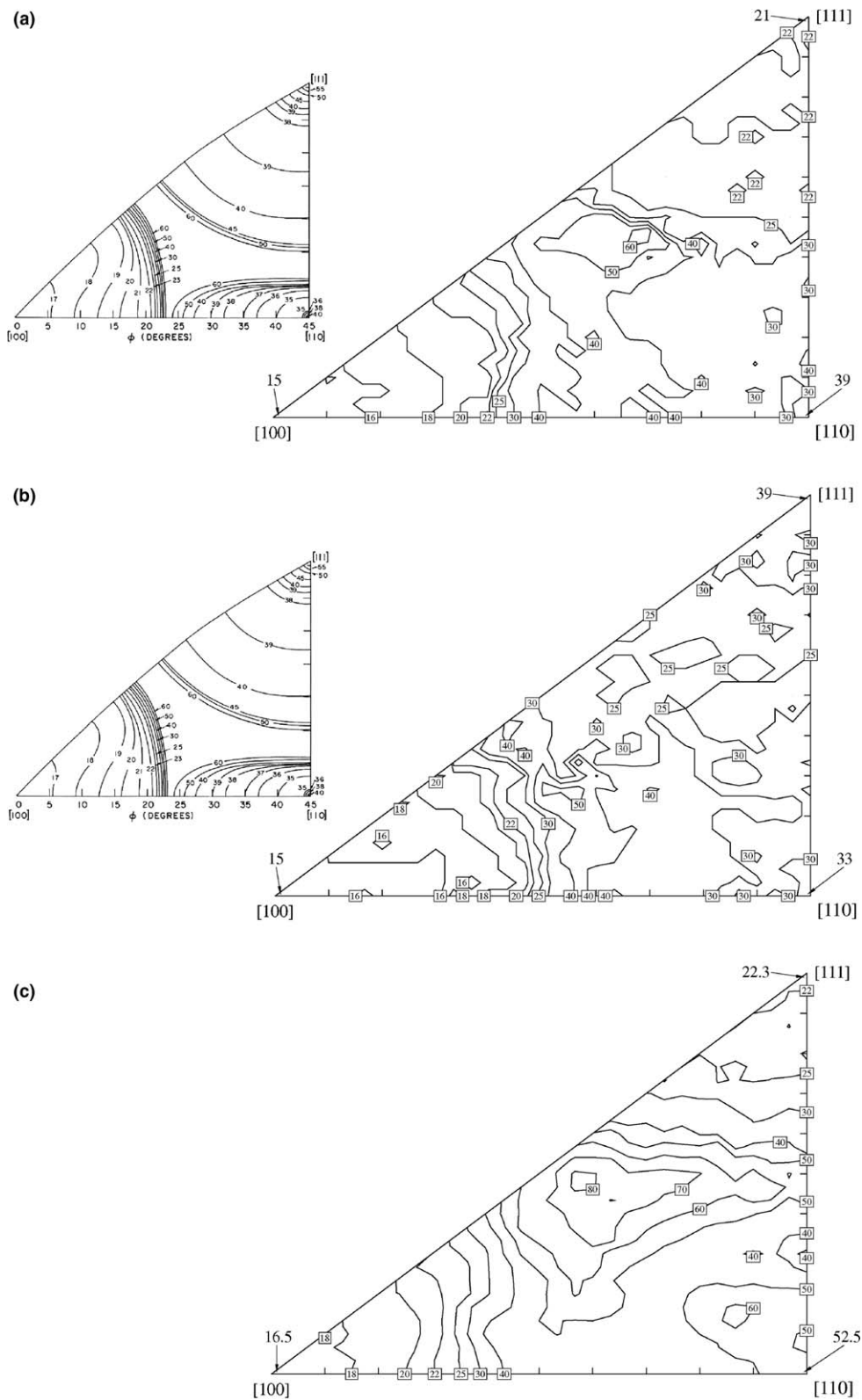
Fig. 6. Contour plots of the three-dimensional threshold displacement energy surface in the triangle of crystallographically non-equivalent crystal directions. Each contour plot is made by first taking the minimum/average of the threshold data in 0.033 Miller index intervals, then making an unsmoothed contour plot. The unit for the threshold curves is eV. The thresholds in the 0.033 Miller index interval from the three principal directions are shown with numbers and arrows: (a) SP-RB potential, minimum of each interval, (b) MHS potential, minimum of each interval and (c) SP-RB potential, average of each interval. The inset in the upper left of figures (a) and (b) shows the original threshold displacement map of Erginsoy et al. [12].

smooth behaviour around the principal 100 direction, while at 110 the threshold very close to the principal direction is in both much larger than just 0.05 Miller indices off it. Also around 111 for the MHS potential a similar behaviour is observed. This explains why the minima for the principal directions differ from those reported in Table 1; note that the values in the table are obtained for Miller index intervals of 0.2.

All three potentials show that the threshold surface close to 100 is flat, that the largest thresholds occur around very roughly the 123 crystal direction, and that a region of larger displacement energies separates the 100 and 110 directions. We checked that also all other potentials show these general features, which clearly are due to simple geometrical reasons independent of the bonding chemistry. No other general trends common to all potential were noted.

Comparison of parts (a) and (c) of Fig. 6 show that when the average instead of the minimum in each interval is considered, a smoother behaviour with similar overall characteristics is observed. It is interesting to note, though, that while the average and minimal values differ only little in the 100 and 111 directions, there is a large difference in the 110 directions. This means that recoils in the 110 direction have for small energies a tiny probability of producing a stable defect, but in most cases a much higher energy is needed to produce a stable defect.

4. Conclusions

We have shown that contrary to a common assumption, the damage production curve as a function of increasing recoil energy for a given atom is not a monotonously rising curve, but can in fact sometimes go to zero after being one already. The probability of this is large enough that it can affect an average threshold significantly.

The methodology used here allows systematic testing of future Fe potentials against threshold displacement experiments.

In our comparison of threshold energies calculated with different potentials, we found that none of the 11 tested potentials agrees fully with experiments, although the SP-RB potential is fairly close. All 11 tested potentials do agree on the following qualitative features: the threshold energy surface $E_d(\theta, \phi)$ close to 100 is flat, the largest threshold energies occur around very roughly the 123 crystal direction, and a region of larger displacement energies separates the 100 and 110 directions.

Acknowledgements

References

[1] M. Burton, J. Phys. Chem. 51 (1947) 611.
[2] F. Seitz, Disc. Faraday Soc. 5 (1949) 271.
[3] M.J. Norgett, M.T. Robinson, I.M. Torrens, Nucl. Engr. Des. 33 (1975) 50.
[4] R.S. Averback, T. Diaz de la Rubia, Displacement damage in irradiated metals and semiconductors, in: H. Ehrenfest, F. Spaepen (Eds.), Solid State Physics, Vol. 51, Academic Press, New York, 1998, p. 281.
[5] R.S. Averback, R. Benedek, K.L. Merkle, Phys. Rev. B 18 (1978) 4158.
[6] D.J. Bacon, T. Diaz de la Rubia, J. Nucl. Mater. 216 (1994) 275.
[7] M. Nastasi, J. Mayer, J. Hirvonen, Ion–Solid Interactions – Fundamentals and Applications, Cambridge University Press, Cambridge, Great Britain, 1996.
[8] H.H. Andersen, Appl. Phys. 18 (1979) 131.
[9] P. Vajda, Rev. Mod. Phys. 49 (1977) 481.
[10] P. Lucasson, The production of Frenkel defects in metals, in: M.T. Robinson, F.N. Young Jr. (Eds.), Fundamental Aspects of Radiation Damage in Metals, Springfield, 1975, p. 42, ORNL.
[11] ASTM Standard E693-94, Standard practice for characterising neutron exposure in iron and low alloy steels in terms of displacements per atom (dpa), 1994.
[12] C. Erginsoy, G.H. Vineyard, A. Englert, Phys. Rev. 133 (1964) A595.
[13] P.G. Lucasson, R.M. Walker, Phys. Rev. 127 (1962) 485.
[14] In the current paper we denote equivalent lattice directions of the type $\langle hkl \rangle$ without the surrounding angle brackets for simplicity.
[15] J.N. Lomer, M. Pepper, Philos. Mag. 16 (1967) 119.
[16] F. Maury, M. Biget, P. Vajda, A. Lucasson, P. Lucasson, Phys. Rev. B 14 (1976) 5303.
[17] M.W. Finnis, J.E. Sinclair, Philps. Mag. A 50 (1984) 45, see also Erratum;
M.W. Finnis, J.E. Sinclair, Philos. Mag. A 53 (1986) 161.
[18] M. Manninen, Phys. Rev. B 34 (1986) 8486.
[19] M.S. Daw, S.M. Foiles, M.I. Baskes, Mater. Sci. Eng. Rep. 9 (1993) 251.
[20] V. Agranovich, V. Kirsanov, Soviet Phys. – Sol. State 12 (1971) 2147.
[21] D.J. Bacon, A.F. Calder, J.M. Harder, S.J. Wooding, J. Nucl. Mater. 205 (1993) 52.
[22] A.F. Calder, D.J. Bacon, J. Nucl. Mater. 207 (1993) 25.
[23] N.V. Doan, R. Vascon, Ann. de Physique C3 20 (Suppl. 3) (1995) 57.
[24] M.I. Haftel, T.D. Andreanis, J. Lill, Phys. Rev. B 42 (1990) 11540.
[25] B.L. Eyre, J. Phys. F: Metal Phys. 3 (1973) 422.
[26] N.W. Ashcroft, N.D. Mermin, Solid State Physics, Saunders College, Philadelphia, 1976.
[27] L. Malerba, J.M. Perlado, Phys. Rev. B 65 (2002) 045202.
[28] F. Maury, P. Vajda, M. Biget, A. Lucasson, P. Lucasson, Radiat. Effects 25 (1975) 175.
[29] H.J.C. Berendsen, J.P.M. Postma, W.F. van Gunsteren, A. DiNola, J.R. Haak, J. Chem. Phys. 81 (1984) 3684.
[30] J.F. Ziegler, J.P. Biersack, U. Littmark, The Stopping and Range of Ions in Matter, Pergamon, New York, 1985.
[31] K. Nordlund, Comput. Mater. Sci. 3 (1995) 448.
[32] K. Nordlund, R.S. Averback, Phys. Rev. B 56 (1997) 2421.
[33] K. Nordlund, M. Ghaly, R.S. Averback, M. Caturla, T. Diaz de la Rubia, J. Tarus, Phys. Rev. B 57 (1998) 7556.
[34] J.P. Biersack, J.F. Ziegler, Nucl. Instr. and Meth. 141 (1982) 93.
[35] D. Terentyev, C. Lagerstedt, P. Olsson, K. Nordlund, J. Wallenius, L. Malerba, J. Nucl. Mater., in press.
[36] L. Malerba, J. Nucl. Mater., in press.
[37] G.J. Ackland, D.J. Bacon, A.F. Calder, T. Harry, Philos. Mag. A Phys. Conden. Matter: Struct., Defects Mech. Properties 75 (1997) 713.

[38] J. Wallenius, P. Olsson, C. Lagerstedt, Nucl. Instr. and Meth. B 228 (2005) 122.

[39] R. Chakarova, V. Pontikis, and J. Wallenius, Delivery Report WP6, SPIRE project, EC contract no. FIKW-CT-2000-00058, 2002. Available from: <http://www.neutron.kth.se/publications>.

[40] M.I. Mendelev, S. Han, D.J. Srolovitz, G.J. Ackland, D.Y. Sun, M. Asta, Philos. Mag. 83 (2003) 3977.

[41] G.J. Ackland, M.I. Mendelev, D.J. Srolovitz, S. Han, A.V. Barashev, J. Phys.: Condens. Matter 16 (2004) S2629.

[42] G. Simonelli, R. Pasianot, E.J. Savino, MRS Symp. Proc. 291 (1989) 567.

[43] C.S. Becquart, C. Domain, A. Legris, J.-C.V. Duysen, J. Nucl. Mater. 280 (2000) 73.

[44] C.S. Becquart, C. Domain, A. Legris, J.-C.V. Duysen, MRS Symp. Proc. 650 (2001) R3.24.1.

[45] A.F.V.R.J. Harrison, S.P. Chen, in: V. Vitek, D.J. Srolovitz (Eds.), Atomistic Simulation of Materials – Beyond Pair Potentials, Plenum, New York, 1989, p. 219.

[46] R.A. Johnson, D.J. Oh, J. Mater. Res. 4 (1989) 1195.

[47] N. Soneda, T. Diaz de la Rubia, Philos. Mag. A. 78 (1998) 995.

[48] M. Ghaly, K. Nordlund, R.S. Averback, Philos. Mag. A 79 (1999) 795.

[49] S.M. Foiles, M.I. Baskes, M.S. Daw, Phys. Rev. B 33 (1986) 7983; Erratum, S.M. Foiles, M.I. Baskes, M.S. Daw, Phys. Rev. B 37 (1988) 10378.

[50] W.H. Press, S.A. Teukolsky, W.T. Vetterling, B.P. Flannery, Numerical Recipes in C; The Art of Scientific Computing, second ed., Cambridge University Press, New York, 1995.

[51] M.P. Allen, D.J. Tildesley, Computer Simulation of Liquids, Oxford University Press, Oxford, England, 1989.

[52] C. Kittel, Introduction to Solid State Physics, third ed., John Wiley and Sons, New York, 1968.

[53] L.A. Girifalco, V.G. Weizer, Phys. Rev. 114 (1959) 687.

[54] C.-C. Fu, F. Willaime, P. Ordejon, Phys. Rev. Lett. 92 (2004) 175503.

[55] F. Banhart, Rep. Prog. Phys. 62 (1999) 1181.

[56] W.A. McKinley Jr., H. Feshbach, Phys. Rev. 74 (1948) 1759.